**Research Article**

# Collider signature of $e^+e^- \to H^+H^-$ in the Scotogenic model

## Nagat A. Elmahdy[1], Asmaa Al-Mellah[2]*, Hakan Akyıldırım[3]

[1]Basic Science Department, Modern Academy for Engineering and Technology, Cairo-Egypt
**Email:** nagat_elmahdy@yahoo.com - **ORCID:** 0000-0002-6152-5842

[2]Süleyman Demirel University, Faculty of Arts & Sciences, Physics Department, 32200, Isparta-Türkiye
**Corresponding Author**: **Email:** asmaa.almellah@gmail.com **ORCID:** 0000-0003-3975-3504

[3]Süleyman Demirel University, Faculty of Arts & Sciences, Physics Department, 32200, Isparta-Türkiye
**Email:** hakanakyildirim@sdu.edu.tr - **ORCID:** 0000-0001-5723-958X

**Abstract:**

We investigate the process $e^+e^- \to H^+H^-$ in the framework of the scotogenic model. The process receives different contributions arising from tree-level diagrams mediated by photon exchange, Z boson exchange and from the exchange of new singlet right-handed fermions $N_{1,2,3}$. We estimate the size of each contribution and the total cross section of the process after applying all dominant constraints on the parameters of the model. We show that the dominant contribution to the cross section originate from the new singlet right-handed fermions $N_{1,2,3}$. Additionally, we show the dependency of the cross section on the centre of mass energy for set of benchmark points of the parameter space of the model respecting the strong obtained bounds. These predictions can be tested in future $e^+e^-$ colliders and hence can test the validity of the model or setting further strong constraints on the model.

## 1. Introduction

The necessity of the presence of New Physics (NP) beyond the standard model (SM) is a consequence of the lack of mechanism to generate neutrino masses in the SM in addition to the absence of Dark Matter (DM) candidate in the SM. Other reasons include the non-inclusion of the gravity in the framework of the SM and the baryon number asymmetry of the Universe that cannot be explained in the SM.

One of the well-known NP beyond the SM is the scotogenic model proposed by Ma in 2006 [1]. The scotogenic Model provides a mechanism for the generation of small neutrino masses favoured by experimental searches. Not only this, but the model also providing a DM candidate that can be any one of the new fermionic or scalar particles proposed by the model. Explicitly, the DM candidate can be a component of $(\eta, N_i)$, $\eta$ is a new scalar doublet, or can be the lightest one of the three singlet Majorana

fermions $N_{1,2,3}$[1]. These are the extra new particles added to the particle content of the SM. It should be noted that a $Z_2$ symmetry is imposed in the model under which all SM particles are even while the new extra particles are odd under this symmetry. In Table 1, we list the quantum numbers of these new extra particles.

*Table 1: Quantum numbers of the new extra particles.*

|  | $N_k$ | $\eta$ |
|---|---|---|
| **SU(2)$_L$** | 1 | 1 |
| **U(1)$_Y$** | 0 | 0 |
| **Z$_2$** | -1 | -1 |

In Ref. [2], the process $e^+e^- \to H^+H^- \to \ell^+\ell'^- \not{E}$ was studied for possible collider signatures. With the progress in the last decade related to neutrino oscillation experiments and different bounds on neutrino masses from some cosmological observations, one can update the previously imposed constraints obtained in that reference. Moreover,

other observations like dark matter relic density measurement have been updated in the last years and thus it turns to be important to include this measurement in the analysis of the model for further possible strong constraints on the model.

Having updated constraints allows us to give correct predictions of the cross section of the process $e^+e^- \longrightarrow H^+H^-$ for which no analysis and predictions were given in Ref. [2]. In fact, our concern about studying the cross section of the process $e^+e^- \longrightarrow H^+H^-$ only as the produced $H^+H^-$ pair can decay to many final states with different combinations of particles. One common effect for all such decay modes is the size of the cross section of $e^+e^- \longrightarrow H^+H^-$. Hence, analysis of this cross section turns to be important. In this study, we do this analysis and investigate the different individual contributions to the cross section that originate from Z, photon and the new singlet fermions proposed by the scotogenic model.

## 2. The scotogenic model

The scotogenic model extends the scalar sector of the SM by adding extra scalar doublet denoted by η. Thus, the Lagrangian describing the scalar sector of the scotogenic model can be written as

$$\mathcal{L} = (\mathcal{D}^\mu\Phi)^\dagger\mathcal{D}_\mu\Phi + (\mathcal{D}^\mu\eta)^\dagger\mathcal{D}_\mu\eta - \mathcal{V} \qquad (1)$$

where $\Phi$ is the SM Higgs doublet, $\mathcal{D}^\mu$ denotes the covariant derivative including the SM gauge fields and the scalar potential $\mathcal{V}$ has the form [1]

$$\mathcal{V} = \mu_1^2\Phi^\dagger\Phi + \mu_2^2\eta^\dagger\eta + \frac{1}{2}\lambda_1(\Phi^\dagger\Phi)^2 + \frac{1}{2}\lambda_2(\eta^\dagger\eta)^2$$
$$+\lambda_3(\Phi^\dagger\Phi)(\eta^\dagger\eta) + \lambda_4(\Phi^\dagger\eta)(\eta^\dagger\Phi)$$
$$+\frac{1}{2}\lambda_5\left[(\Phi^\dagger\eta)^2 + (\eta^\dagger\Phi)^2\right]$$

Upon electroweak symmetry breaking, we can write

$$\Phi = \begin{pmatrix} 0 \\ \frac{1}{\sqrt{2}}(h+v) \end{pmatrix}, \quad \eta = \begin{pmatrix} H^+ \\ \frac{1}{\sqrt{2}}(\mathcal{S} + i\mathcal{P}) \end{pmatrix} \qquad (2)$$

where h stands for the physical Higgs boson and v represents the vacuum expectation value (VEV) of $\Phi$. One of the consequences of the $Z_2$ symmetry is that the VEV of η is zero. The scalar particles masses are given as $m_S^2 = m_\mathcal{P}^2 + \lambda_5 v^2 = \mu_2^2 + \frac{1}{2}(\lambda_3 + \lambda_4 + \lambda_5)v^2$ and $m_H^2 = \mu_2^2 + \frac{1}{2}\lambda_3 v^2$ [2]. In the limit of

very small $\lambda_5$ [3], $|\lambda_5| \ll |\lambda_3 + \lambda_4|$, one finds that, $m_S^2 \simeq m_\mathcal{P}^2$.

The masses and interactions of the new singlet Majorana fermions, $N_k$, can be inferred from the following Lagrangian

$$\mathcal{L}_N = -\frac{1}{2}M_k\overline{N_k^c}P_R N_k +$$
$$\mathcal{Y}_{rk}\left[\bar{\ell}_r H^- - \frac{1}{\sqrt{2}}\bar{\nu}_r(S - i\mathcal{P})\right]P_R N_k + \text{H.c.}, \qquad (3)$$

with $\ell_{1,2,3} = e, \mu, \tau, \mathcal{Y}_{rk}$ and $M_k$ denote the Yukawa couplings and masses of $N_k$, and the superscript c refers to the charge conjugation of the field. In the above equation, we have $P_R = \frac{1}{2}(1 + \gamma_5)$ and $k, r = 1,2,3$. The interactions of $H^\pm$ with photon $A$, and $Z$ boson relevant to our process can be obtained from the Lagrangian $\mathcal{L}_H^\pm$ that can be expressed as

$$\mathcal{L}_H^\pm \supset ie(H^+\partial^\rho H^- - H^-\partial^\rho H^+)A_\rho$$
$$+ \frac{g}{2c_w}[i(1 - 2s_w^2)(H^+\partial^\rho H^-$$
$$- H^-\partial^\rho H^+)]Z_\rho$$
$$(4)$$

where $e = gs_w$ is the electromagnetic charge, $c_w = \cos\theta_w$ and $s_w = \sin\theta_w$ with $\theta_w$ being the Weinberg angle.

### 2.1 Neutrino masses generation

Due to the imposed $Z_2$ symmetry, neutrinos masses cannot exist at the tree level in the scotogenic model. This is not the case at one loop level where neutrinos masses can be generated through $S$, $\mathcal{P}$, and $N_k$ mediating the loop. The mass eigenvalues of the light neutrinos $m_i$ can be obtained using the loop generated quantity [1]

$$\Lambda_k = \frac{\lambda_5 v^2}{16\pi^2 M_k}\left[\frac{M_k^2}{m_0^2 - M_k^2} + \frac{2M_k^4 \ln(M_k/m_0)}{(m_0^2 - M_k^2)^2}\right] \qquad (5)$$

Here $m_0 = \frac{1}{2}(m_S + m_\mathcal{P}) \simeq m_S \simeq m_\mathcal{P}$. The neutrino mass matrix then becomes

$$\mathcal{M}_v = Y\,\text{diag}(\Lambda_1, \Lambda_2, \Lambda_3)Y^T, \qquad (6)$$

which can be diagonalized using

$$\text{diag}(m_1, m_2, m_3) = \mathcal{U}^\dagger\mathcal{M}_v\mathcal{U}^*, \qquad (7)$$

The unitary matrix $U$ denotes the well-known Pontecorvo-Maki-Nakagawa-Sakata (PMNS) matrix. In our study we use the PDG parametrization [4] $\mathcal{U} = \tilde{u}\,\text{diag}(e^{i\alpha_1/2}, e^{i\alpha_2/2}, 1)$, where $\alpha_{1,2}$ denoting

the Majorana CP-violation phases and the matrix $\tilde{u}$ is expressed in terms of $c_{mn} = \cos\theta_{mn} \geq 0$, $s_{mn} = \sin\theta_{mn} \geq 0$ and a Dirac phase $\delta$. The expression of the matrix $\tilde{u}$ can be found in Eq. (10) in Ref. [5]. Analytic solutions for Eqs. (7) yield [2]

$$Y_{e1} = \frac{-c_{12}c_{13}Y_1}{c_{12}c_{23}s_{13}e^{i\delta} - s_{12}s_{23}},$$
$$Y_{e2} = \frac{-s_{12}c_{13}Y_2}{s_{12}c_{23}s_{13}e^{i\delta} + c_{12}s_{23}},$$

$$Y_{\mu1} = \frac{(c_{12}s_{23}s_{13}e^{i\delta} + s_{12}c_{23})Y_1}{c_{12}c_{23}s_{13}e^{i\delta} - s_{12}s_{23}}, \quad Y_{\mu3} = \frac{s_{23}Y_3}{c_{23}},$$

$$Y_{e3} = \frac{s_{13}Y_3}{c_{23}c_{13}e^{i\delta}}, \quad Y_{\mu2} = \frac{(s_{12}s_{23}s_{13}e^{i\delta} - c_{12}c_{23})Y_2}{s_{12}c_{23}s_{13}e^{i\delta} + c_{12}s_{23}},$$
$$Y_{\tau k} = Y_k \,, \tag{8}$$

which correspond to the light neutrino mass eigenvalues [2]

$$m_1 = \frac{\Lambda_1 Y_{e1}^2 e^{-i\alpha_1}}{c_{12}^2 c_{13}^2}, m_2 = \frac{\Lambda_2 Y_{e2}^2 e^{-i\alpha_2}}{s_{12}^2 c_{13}^2}, m_3 = \frac{\Lambda_3 Y_3^2}{c_{13}^2 c_{23}^2} \tag{9}$$

The Majorana CP-violation phases can be calculated with the help of the following relations.

$$\alpha_1 = \arg(\Lambda_1 Y_{e1}^2), \alpha_2 = \arg(\Lambda_2 Y_{e2}^2), \arg(\Lambda_3 Y_3^2) = 0 \tag{10}$$

## 2.2 Dark Matter

The scotogenic model enlarges particle contents of the fermionic and scalar sectors of the SM through introducing the new particles $N_{1,2,3}$ and $S, P, H^{\pm}$ respectively. These new particles are odd under $Z_2$ symmetry and hence the lightest one among them will be stable and can be a DM candidate.

In our study we consider the familiar scenario in which $N_1$ is the DM particle and the second lightest particle $N_2$ is degenerate in mass with $N_1$. This scenario is favored as it ensures the ability of satisfying simultaneously the constraints from the DM relic density and the Branching ratio (BR) of the lepton flavour violation process $\mu \to e\gamma$.

The relic density can be expressed in terms of the present DM density relative to its critical value, denoted by $\Omega$, and the Hubble parameter, denoted by $\hat{h}$, as $\Omega\hat{h}^2$. Theoretically, it can be estimated from the relation [3, 6]

$$\Omega\hat{h}^2 = \frac{1.07 \times 10^9 x_f \, GeV^{-1}}{\sqrt{g_*} m_{P1}[a_{eff} + 3(b_{eff} - a_{eff}/4)/x_f]}$$

$$x_f = \ln \frac{0.191(a_{eff} + 6b_{eff}/x_f)M_1 \, m_{P1}}{\sqrt{g_* x_f}} \tag{11}$$

here $g_*$ is the number of relativistic degrees of freedom below the freeze-out temperature $T_f = M_1/x_f$ and $m_{P1} = 1.22 \times 10^{19}$ GeV is the Planck mass. The expressions of $a_{eff}$ and $b_{eff}$ can be inferred from the expansion of the coannihilation rate $\sigma_{eff}v_{rel} = a_{eff} + b_{eff}v_{rel}^2$ where the expansion is performed in terms of the relative speed of the annihilating particles in their center-of-mass frame denoted by $v_{rel}$ and $\sigma_{eff} = \frac{1}{4}(\sigma_{11} + \sigma_{12} + \sigma_{21} + \sigma_{22})$. The expression of $\sigma_{ij}$, for $i, j = 1, 2$, can be obtained from the relation.

$$\sigma_{ij} = \sigma_{N_i N_j \to \ell_i^- \ell_j^+} + \sigma_{N_i N_j \to v_i v_j} \tag{12}$$

Above cross sections were computed in Refs. [7, 2] and each arises from the t and u channels tree-level diagrams mediated by the exchange of $H^{\pm}$ and (S, P) depending on whether the final states are charged leptons or neutral neutrinos.

In our analysis of the resultant constraint, from the measured value of the DM relic density, on the parameter space of the model under concern we consider the case that the DM and the new scalar particles are not degenerate in mass to avoid the contributions of the coannihilation processes of the scalars to the relic density.

## 2.3 $e^+(p_+)e^-(p_-) \longrightarrow H^+H^-$

In the scotogenic model under the study in this work, the amplitude of the process $e^+(p_+)e^-(p_-) \to H^+H^-$ receive contributions from the tree-level diagrams mediated by the exchange of photon $(\gamma)$, Z and $N_{1,2,3}$ diagrams. In the limit of massless $e^{\pm}$, the resulting cross section is given as [2]

$$\sigma_{e^+e^- \to H^+H^-} = \frac{\pi\alpha^2\beta^3}{3s} + \frac{\alpha}{12}\frac{(g_L^2 + g_L g_R)\beta^3}{s - m_Z^2} +$$

$$\frac{(g_L^4 + g_L^2 g_R^2)\beta^3 s}{96\pi(s - m_Z^2)^2} + \sum_k \frac{|y_{1k}|^4}{64\pi s}\left(\omega_k \ln\frac{\omega_k + \beta}{\omega_k - \beta} - 2\beta\right) +$$

$$\left[\frac{\alpha}{16s} + \frac{g_L^2}{64\pi(s - m_Z^2)}\right]\sum_k|y_{1k}|^2\left[(\omega_k^2 - \beta^2)\ln\frac{\omega_k + \beta}{\omega_k - \beta} -\right.$$

$$\left. 2\beta\omega_k\right] + \sum_{j,k>j}\frac{|y_{1j}y_{1k}|^2}{64\pi s}\left(\frac{\omega_j^2 - \beta^2}{\omega_j - \omega_k}\ln\frac{\omega_j + \beta}{\omega_j - \beta} +\right.$$

$$\left. \frac{\omega_k^2 - \beta^2}{\omega_k - \omega_j}\ln\frac{\omega_k + \beta}{\omega_k - \beta} - 2\beta\right) \tag{13}$$

here $j, k = 1, 2, 3$, $s = (p_+ + p_-)^2$, $\alpha = \frac{e^2}{4\pi}$, $\beta = \sqrt{1 - \frac{4m_H^2}{s}}$ and $\omega_k = 1 + \frac{2M_k^2}{s} - \frac{2m_H^2}{s} > \beta$ . In the numerical analysis, we employ the effective values $\alpha = 1/128$, g = 0.6517, and $s_w^2 = 0.23146$ [4].

## 2.4 Constraints

In our study, we adopt the normal ordering (NO) of neutrino masses. The mixing angles, the Dirac phase, $|\Delta m_{31}^2|$ and $|\Delta m_{21}^2|$ can be determined from various measurements. In our numerical evaluation, we employ the results of the fit to the global data on neutrino oscillations carried out in Ref. [8]. Using the results of the fit allows us to impose the constraint $32.0 < Rm \equiv \frac{|\Delta m_{31}^2|}{\Delta m_{21}^2} < 36.0$ on the parameter space based on the 90% $CL$ ranges of the data. On the other hand, the CMB temperature, polarization and lensing measurements from the Planck satellite, BAO observations, $H(z)$ information and Supernovae Ia data constraint result in the stringent $2\sigma$ upper limit $\sum m_i < 0.12$eV. Possible constraints can be derived from Neutrinoless double beta decay experiments. The resulted constraint reads $|\langle m \rangle_{ee}| < 0.06 - 0.2$eV at the 95% confidence level [9, 10, 11] where $\langle m \rangle_{ee}$ is defined as $\langle m \rangle_{ee} = m_1 \mathcal{U}_{e1}^2 + m_2 \mathcal{U}_{e2}^2 + m_3 \mathcal{U}_{e3}^2$.

The Yukawa interactions including the charged Higgs $H^\pm$ listed in Eq. (3) can generate one loop-level diagrams that contribute to the lepton flavour violation (LFV) processes. A detailed discussion of these process can be found in Ref. [12]. Currently, the experimental upper bounds on the branching ratios of a class of these processes are BR($\mu \to e\gamma$) $< 4.2 \times 10^{-13}$ [13], BR($\tau \to e\gamma$) $< 3.3 \times 10^{-8}$ [14], and BR($\tau \to \mu\gamma$) $< 4.4 \times 10^{-8}$ [14] with the most stringent constraint come from BR($\mu \to e\gamma$). The expressions of the branching ratios of these LFV processes in the framework of the scotogenic model can be found in Ref. [12]. On the other hand, the flavour-diagonal counterpart of the aforementioned LFV processes can modify the anomalous magnetic moment, $a_{\ell_i}$, as [15]

$$\Delta a_{\ell_i} = \frac{-m_{\ell_i}^2}{16\pi^2 m_H^2} \sum_k |Y_{ik}|^2 \mathcal{F}(M_k^2/m_H^2) \qquad (14)$$

It turns out that, the anomalous magnetic moment of the muon yields a stronger bound compared to the

others, electron and tau, on the scotogenic parameter space. The difference between the SM prediction and the currently experimental value of $a_\mu$ reads $a_\mu^{exp} - a_\mu^{SM} = (2.51 \pm 0.59) \times 10^{-9}$ [16].

Direct detection of DM through the interaction of $N_1$ with nucleons, resulting from the Higgs exchange at the one-loop level, was discussed in Ref. [17]. To avoid the stringent constraints from direct detection [18, 19], we can follow Ref. [17, 20] and take $\lambda_{3,4} = 0.01$. This has a consequence that $m_o \simeq m_{H^\pm} + \frac{1}{2}\lambda_4 v^2 \simeq m_{H^\pm} + 350\ GeV$. One should remark that the strong bounds from the direct detection were not taken into account in Refs. [2]. In this study we take these bounds into account and employ the latest neutrino oscillation data obtained as a result of the global analysis presented in Ref. [8]. In the next section, we will present our results and will give our analysis and discussion of these results. To do this, we first set the mixing angles $\theta_{12,23,13}$ and the Dirac phase $\delta$ to their central values obtained in the fit to the global data on neutrino oscillations performed in Ref. [8]. In the second step, we perform a scan over the parameter space of the model namely, the masses of the new scalars $m_H, m_o$ and the new singlet fermions $N_{1,2,3}$ and the input parameters $Y_{1,2,3}$ appearing in the Yukawa couplings listed above in Eq. (8). For light dark matter masses $M_1 < 100\ GeV$, lepton flavor violation [21] and direct search at LHC [22, 23] mostly exclude the parameter space. Concerning the scalar masses, using the data on W and Z widths and the null results of direct searches for new particles at $e^+e^-$colliders we have the following upper bounds on the scalar masses [24, 25, 26]

$$m_{H^\pm} + m_{S,\mathcal{P}} > m_{W^\pm}, \ m_{H^\pm} > 70\ GeV, m_S + m_{\mathcal{P}} > m_Z \qquad (15)$$

One should remark that there are constrains on the charged Higgs mass from the $B \to \tau\nu$, $B \to s\gamma$ and from the direct measurements of the charged Higgs decays at the LHC. In our analysis, we take into account all these constraints.

## 3. Results and Discussions

We start our analysis by showing the allowed regions in the parameter space of the scotogenic

model upon applying the most stringent constraints individually and then simultaneously.
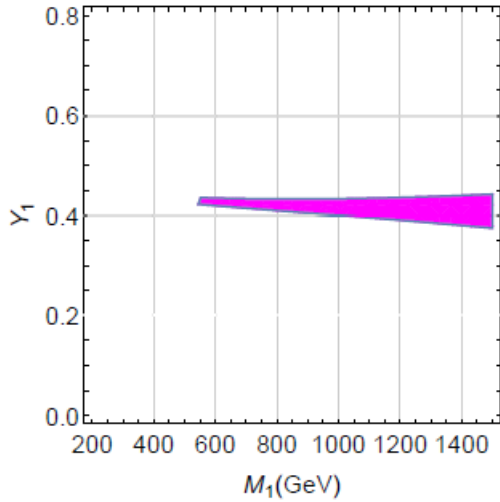


**Figure 1.** *Region in magenta colour is allowed by* $\mu \rightarrow e\gamma$ *constraint for the parameters* $M_2 = M_1$, $M_3 = M_1 + 380\ GeV$, $m_H = M_1 + 400\ GeV$, $Y_2 = 0.49$ *and* $Y_3 = 0.66$.

In Fig.1, the region in magenta colour is allowed by $\mu \rightarrow e\gamma$ constraint where we fixed the other parameters as $M_2 = M_1$, $M_3 = M_1 + 380\ GeV$, $m_H = M_1 + 400\ GeV$, $Y_2 = 0.49$ and $Y_3 = 0.66$. Clearly from the figure that, satisfying $\mu \rightarrow e\gamma$ constraint requires large charged Higgs mass and also large $N_{1,2,3}$ masses.
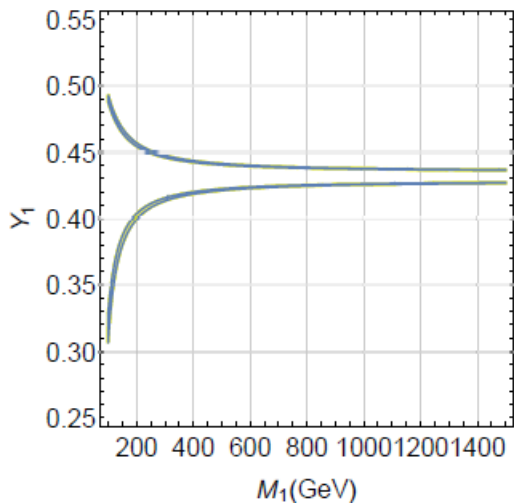


**Figure 2.** *Allowed regions after imposing* $\frac{|\Delta m_{31}^2|}{\Delta m_{21}^2}$ *constraints for the choice of the parameters as* $M_2 = M_1$, $M_3 = M_1 + 380\ GeV$, $m_o = M_1 + 750\ GeV$, $Y_2 = 0.49$ *and* $Y_3 = 0.66$.

In Fig.2, we display the allowed regions after taking into account the imposed $\frac{|\Delta m_{31}^2|}{\Delta m_{21}^2}$ constraint. In the

figure we set the parameters as $M_2 = M_1$, $M_3 = M_1 + 380\ GeV$, $m_o = M_1 + 750\ GeV$, $Y_2 = 0.49$ and $Y_3 = 0.66$. The colored regions in the $M_1 - Y_1$ plane satisfy the desired constraint.

We turn now to display the allowed region in the $M_1 - Y_1$ plane by the DM relic density $\Omega \hat{h}^2$ constraints. Our result is presented in Fig.3 for the set of the parameters $M_2 = M_1$, $M_3 = M_1 + 380\ GeV$, $m_H = M_1 + 400\ GeV$, $m_o = M_1 + 750\ GeV$, $Y_2 = 0.49$ and $Y_3 = 0.66$. As can be seen from the figure that, large values of DM masses $M_1$ require large values of the parameter $Y_1$ to satisfy the constraint. This requirement is not favored by the other constraints discussed above. It should be noted that, in the previous figures presented above we discussed the effect of each individual constraint on the parameter space. However, the parameter space must be subjected to all strong constraints at the same time. Consequently, in Fig.4, we show our results for the allowed region in the $M_1 - Y_1$ plane by the dominant constraints arising from $\mu \rightarrow e\gamma$, $\frac{|\Delta m_{31}^2|}{\Delta m_{21}^2}$, and $\Omega \hat{h}^2$. The green colour region in the figure simultaneously satisfies all these constraints simultaneously. We deduce from this region that; it is possible to have points satisfying all constraints for masses of the new particles in the model with masses close to or higher than 1 TeV. Moreover, we can use this region to obtain set of benchmark points that satisfy the imposed constraints on the parameter space of the model and hence can give a prediction of the model to the cross section of $\sigma_{e^+e^- \rightarrow H^+H^-}$ which can be tested in future colliders.
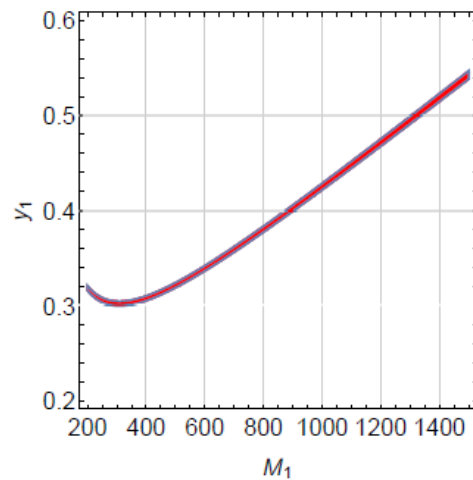


**Figure 3.** *Allowed regions in the* $M_1 - Y_1$ *plane by* $\Omega \hat{h}^2$ *constraints for the parameters* $M_2 = M_1$, $M_3 = M_1 + 380\ GeV$, $m_H = M_1 + 400\ GeV$, $m_o = M_1 + 750\ GeV$, $Y_2 = 0.49$ *and* $Y_3 = 0.66$.
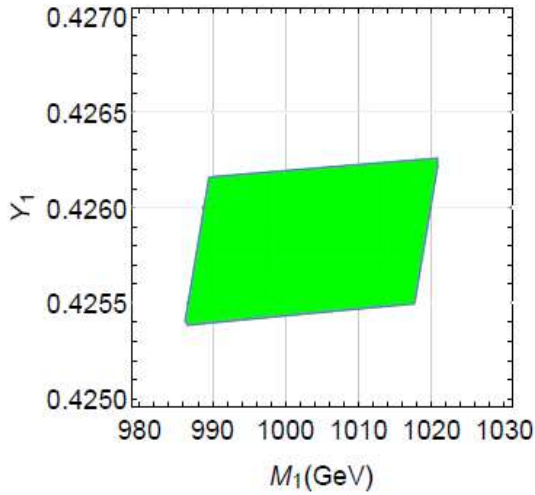
**Figure 4.** *Allowed regions in the $M_1 - Y_1$ plane by $\mu \to e\gamma$, $\frac{|\Delta m_{31}^2|}{\Delta m_{21}^2}$, $\Omega \hat{h}^2$ constraints for the parameters $M_2 = M_1$, $M_3 = M_1 + 380\ GeV$, $m_H = M_1 + 400\ GeV$, $m_o = M_1 + 750\ GeV$, $Y_2 = 0.49\ and\ Y_3 = 0.66$.*

In Fig.5, we show our results for the individual contributions of Z, photon and new singlet fermions $N_{1,2,3}$ to the cross section of $\sigma_{e^+e^- \to H^+H^-}$ as a function of the centre of mass energy $\sqrt{s}$ in red, orange and magenta colors respectively. The plots in the figure correspond to the one of the allowed benchmark points of the parameter space namely $M_1 = 1005\ GeV$, $M_2 \simeq M_1 = 1005.0000035\ GeV$, $M_3 = 1385\ GeV$, $m_H = 1405\ GeV$, $Y_1 = 0.4258$, $Y_2 = 0.49$ and $Y_3 = 0.66$. Clearly from the figure that Z contribution to the cross section is the least one while contributions from the new singlet fermions $N_{1,2,3}$ are the dominant ones. It should be noted from the figure that we extended the center of mass energies to higher values and that the prospective ILC has an upper limit of 1 TeV and the CLIC has an upper limit to 3 TeV. Our objective, doing so, is to cover large ranges of energies that can be tested in any future collider with much higher center of mass energies than ILC and CLIC.

Finally, in Fig.6, we show our results for the total cross section of $\sigma_{e^+e^- \to H^+H^-}$ as a function of the centre of mass energy $\sqrt{s}$ in red, orange and magenta colors respectively. As above, the figure correspond to the one of the allowed benchmark points of the parameter space namely $M_1 = 1005\ GeV$, $M_2 \simeq M_1 = 1005.0000035\ GeV$, $M_3 = 1385\ GeV$, $m_H = 1405\ GeV$, $Y_1 = 0.4258$, $Y_2 = 0.49$ and

$Y_3 = 0.66$. As can be seen from the figure that, the cross section increases with increasing the centre of mass energy till it reach to its beak and then starting to decrease with increasing the centre of mass energy.
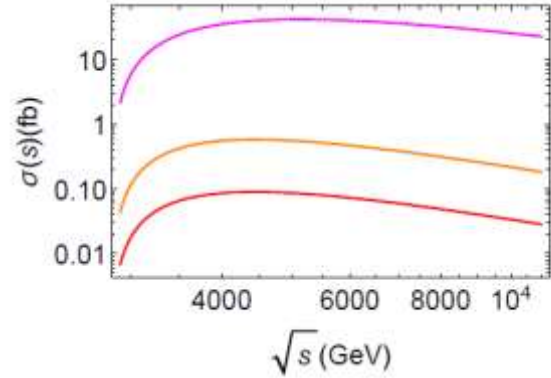


**Figure 5.** *Z, photon, and new singlet fermions $N_{1,2,3}$ individual contributions to the cross section of $\sigma_{e^+e^- \to H^+H^-}$ in red, orange, and magenta colours respectively. The plots correspond to the allowed parameters $M_1 = 1005\ GeV$, $M_2 \simeq M_1 = 1005.0000035\ GeV$, $M_3 = 1385\ GeV$, $m_H = 1405\ GeV$, $Y_1 = 0.4258$, $Y_2 = 0.49\ and\ Y_3 = 0.66$.*
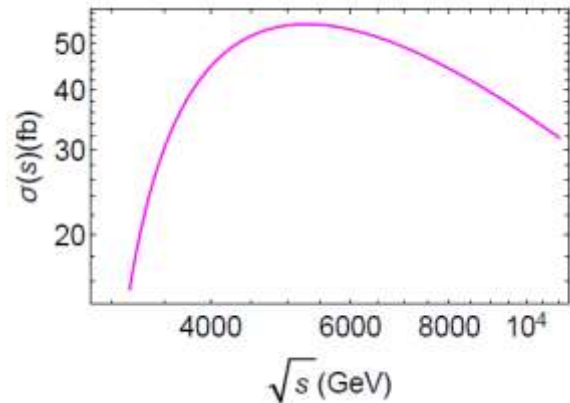


**Figure 6.** *Total cross section $\sigma_{e^+e^- \to H^+H^-}$. The plots correspond to the allowed parameters $M_1 = 1005\ GeV$, $M_2 \simeq M_1 = 1005.0000035\ GeV$, $M_3 = 1385\ GeV$, $m_H = 1405\ GeV$, $Y_1 = 0.4258$, $Y_2 = 0.49\ and\ Y_3 = 0.66$.*

## 4. Conclusions

In this work we have studied the process $e^+e^- \to H^+H^-$ in the Scotogenic model. The different contributions to the amplitude of the process originate from tree-level diagrams mediated by photon, Z boson and from the right-handed fermions $N_{1,2,3}$. We have studied the processes that can impose strong constraints on the parameter space relevant to the process $e^+e^- \to H^+H^-$. Moreover, we have estimated the size of the individual contributions of each of photon, Z boson and the

right-handed fermions $N_{1,2,3}$ to the cross section of $e^+e^- \rightarrow H^+H^-$ after taking into account all stringent constraints on the parameters of the model.

We have shown that the main contribution to the cross section arise from the new singlet right-handed fermions $N_{1,2,3}$. Finally, we have shown the dependency of the cross section on the centre of mass energy for set of benchmark points of the parameter space of the model respecting the strong obtained bounds. Future $e^+e^-$ colliders will search for the process $e^+e^- \rightarrow H^+H^-$ and thus can test our predictions for either setting more stringent constraints or verifying these predictions.

## Author Statements:

- **Ethical approval:** The conducted research is not related to either human or animal use.
- **Conflict of interest:** The authors declare that they have no known competing financial interests or personal relationships that could have appeared to influence the work reported in this paper
- **Acknowledgement:** The authors declare that they have nobody or no-company to acknowledge.
- **Author contributions:** The authors declare that they have equal right on this paper.
- **Funding information:** The authors declare that there is no funding to be acknowledged.
- **Data availability statement:** The data that support the findings of this study are available on request from the corresponding author. The data are not publicly available due to privacy or ethical restrictions.

## References

[1] E. Ma. (2006). Verifiable radiative seesaw mechanism of neutrino mass and dark matter.*Physical Review D.* 73: 077301. DOI:10.1103/PhysRevD.73.077301.

[2] S. Y. Ho &amp; J. Tandean. (2014). Probing ScotogenicEffects in Colliders. *Physical Review. D.* 89:114025. DOI: 10.1103/PhysRevD.89.114025.

[3] J. Kubo, E. Ma &amp; D. Suematsu. (2006). Cold Dark Matter, Radiative Neutrino Mass, μ→e, and Neutrino less Double β Decay. *Physical Letter B.* 642:18-23. DOI: 10.1016/j.physletb.2006.08.085.

[4] J. Beringer et al., (2012). Review of Particle Physics (RPP). *Physical Review D.* 86:010001. DOI:i:10.1103/PhysRevD.86.010001.

[5] G. Faisel, S. Y. Ho &amp; J. Tandean, (2014). Exploring X-ray lines as scotogenic signals. *Physics Letters B.* 738:380-385. DOI:10.1016/j.physletb.2014.09.063.

[6] G. Jungman, M. Kamionkowski, &amp; K. Griest, (1996). Supersymmetric dark matter. *Physics Reports.* 267(5–6): 195-373. DOI:10.1016/0370-1573(95)00058-5.

[7] S. Y. Ho &amp; J. Tandean, (2013). Probing Scotogenic effects in Higgs Boson Decays. *Physical Review D.* 87:095015. DOI:10.1103/PhysRevD.87.095015.

[8] P. F. de Salas et al., (2021). 2020 global reassessment of the neutrino oscillation picture. *Journal of High Energy Physics.* 02:071. DOI:10.1007/JHEP02(2021)071.

[9] G. Anton et al., (2019). Search for Neutrino less Double-β Decay with the Complete EXO-200 Dataset. *Physical. Review Letter.* 123(16): 161802. DOI:10.1103/PhysRevLett.123.161802.

[10] A. Gando et al., (2016). Search for Majorana Neutrinos near the Inverted Mass Hierarchy Region with KamLAND-Zen. *Physical Review Letter.* 117(8): 082503. DOI:10.1103/PhysRevLett.117.082503.

[11] M. Agostini et al., (2020). Final Results of GERDA on the Search for Neutrino less Double-β Decay. *Physical Review Letter.* 125(25): 252502. DOI:10.1103/PhysRevLett.125.252502.

[12] T. Toma &amp; A. Vicente. (2014). Lepton flavour violation in the scotogenic model. *Journal of High Energy Physics.* 2014(1):1-27. DOI:https://doi.org/10.48550/arXiv.1312.2840.

[13] A. M. Baldini et al., (2016). Search for the lepton flavour violating decay → with the full dataset of the MEG experiment. *European Physics J. C.* 76(8):434. DOI: 10.1140/epjc/s10052-016-4271-x.

[14] B. Aubert et al., (2010). Searches for Lepton Flavor Violation in the Decays →γ and →γ. *Physical Review Letter.* 104:021802. DOI:10.1103/PhysRevLett.104.021802.

[15] E. Ma &amp; M. Raidal. (2001). Neutrino mass, muon anomalous magnetic moment, and lepton flavor non conservation. *Physical Review Letter.* 87:011802. DOI: 10.1103/PhysRevLett.87.011802.

[16] T. Aoyama, et al., (2020). The anomalous magneticmoment of the muon in the Standard Model. *Physics Report* 887:1-166. DOI:10.1016/j.physrep.2020.07.006.

[17] A. Ibarra, C. E. Yaguna &amp; O. Zapata. (2016). Direct Detection of Fermion Dark Matter in the Radiative Seesaw *Model. Physical Review D.* 93(3): 035012.DOI:10.1103/PhysRevD.93.035012.

[18] E. Aprile et al., (2018). Dark Matter Search Results from a One Ton-Year Exposure of XENON1T. *Physical Review Letter.* 121(11): 111302. DOI: 10.1103/PhysRevLett.121.111302.

[19] Y. Meng et al., (2021). Dark Matter Search Results from the PandaX-4T Commissioning Run. *Physical Review Letter.* 127(26): 261802. DOI:10.1103/PhysRevLett.127.261802.

[20] Jiao Liu et al. (2022). Unraveling the Scotogenic model at muon collider. *Journal of High Energy Physics.* 12(57):001-034

[21] A. Vicente &amp; C. E. Yaguna. (2015). Probing the scotogenic model with lepton flavor violating

processes. *Journal of High Energy Physics*. 2015(2):144-150. DOI: 10.1007/JHEP02(2015)144.

[22] G. Aad et al., (2020). Searches for electroweak production of supersymmetric particles with compressed mass spectra in =13 TeV pp collisions with the ATLAS detector. *Physical Review D.* 101(5): 052005. DOI: 10.1103/PhysRevD.101.052005.

[23] A. M. Sirunyan et al., (2021). Search for supersymmetry in final states with two oppositely charged same-flavor leptons and missing transverse momentum in proton-proton collisions at =13 TeV. *Journal of High Energy Physics.* 04:123. DOI:10.1007/JHEP04(2021)123.

[24] A. Arhrib, R. Benbrik, &amp; N. Gaur. (2012). H→ in Inert Higgs Doublet Model. *Physical Review D.* 85:095021. DOI: 10.1103/PhysRevD.85.095021.

[25] Q.H. Cao, E. Ma, &amp; G. Rajasekaran. (2007). Observing the Dark Scalar Doublet and its Impact on the Standard-Model Higgs Boson at Colliders. *Physical Review D.* 76:095011. DOI: 10.1103/PhysRevD.76.095011.

[26] Dolle, Ethan M. and Su, Shufang. (2022) Inert dark matter, *Physical Review D.* 5(80): 1550-2368. DOI:10.1103/physrevd.80.055012.